

Vortex States in Archimedean Tiling Pinning Arrays

D. Ray^{1,2}, C. Reichhardt¹, and C. J. Olson Reichhardt¹

¹ Theoretical Division, Los Alamos National Laboratory, Los Alamos, New Mexico 87545 USA

² Department of Physics, University of Notre Dame, Notre Dame, Indiana 46556

E-mail: cjr@lanl.gov

Abstract. We numerically study vortex ordering and pinning in Archimedean tiling substrates composed of square and triangular plaquettes. The two different plaquettes become occupied at different vortex densities, producing commensurate peaks in the magnetization at non-integer matching fields. We find that as the field increases, in some cases the fraction of occupied pins can decrease due to the competition between fillings of the different plaquette types. We also identify a number of different types of vortex orderings as function of field at integer and non-integer commensurate fillings.

PACS numbers: 74.25.Wx, 74.25.Uv

1. Introduction

There have been extensive studies on vortex ordering and pinning for superconductors with periodic arrays of pinning sites where the arrays have square or triangular order. In these systems the critical current or the force needed to depin the vortices passes through maxima due to commensuration effects that occur when the number of vortices is an integer multiple of the number of pinning sites [1, 2, 3, 4, 5, 6, 7, 8]. The field at which the number of vortices equals the number of pinning sites is labeled B_ϕ , so that commensurate peaks arise at $B/B_\phi = n$, where n is an integer. At these matching fields various types of vortex crystalline states can form as has been directly observed in experiments and confirmed in simulations [9, 10, 11, 12]. It is also possible for fractional matching commensurability effects to occur at fillings of $B/B_\phi = n/m$, where n and m are integers. For square and triangular arrays, these fractional matching peaks are typically smaller than the integer matching peaks. The fractional matchings are associated with different types of ordered or partially ordered vortex arrangements [13, 14, 15, 16, 17].

In studies of rectangular pinning arrays, a crossover from matching of the full two-dimensional (2D) array to matching with only one length scale of the array occurs for increasing field [18, 19]. Honeycomb and kagome pinning arrays [20, 21, 22, 23, 24] are constructed by the systematic dilution of a triangular pinning array. In a honeycomb array, every third pinning site of the triangular array is removed, while for a kagome array, every fourth pinning site is removed. In these systems there are strong commensurability effects at both integer and noninteger matching fields, where the noninteger matchings correspond to integer matchings of the original undiluted triangular array. A similar effect can occur for the random dilution of a triangular pinning lattice, where commensuration effects occur at integer matching fields as well as at the noninteger matching fields corresponding to the integer matching fields of the original undiluted pinning array [25, 26]. Other periodic pinning array geometries have also been studied which have artificial vortex spin ice arrangements [27] or composite arrays of smaller and larger coexisting pinning sites [28, 29].

Here we propose and study new types of periodic pinning geometries that can be constructed from Archimedean tilings of the plane. In contrast to a regular tiling where a single type of regular polygon (such as a square or equilateral triangle) is used to tile the plane, an Archimedean tiling uses two or more different polygon types. We consider two examples of Archimedean tilings constructed with a combination of square and triangular plaquettes, the elongated triangular tiling illustrated in figure 1(b), and the snub square tiling shown in figure 1(c). The plaquettes around one vertex in each tiling are highlighted with dotted lines and marked with the number of sides. The tilings are named by reading off the number of sides in a clockwise order around the pinning site, giving 33344 (also written as 3^34^2) for the tiling in figure 1(b), and 33434 (or 3^2434) for the tiling in figure 1(c). In figure 2 one can see the basis of plaquettes for each tiling which is translated in order to generate the full tiling. For each tiling,

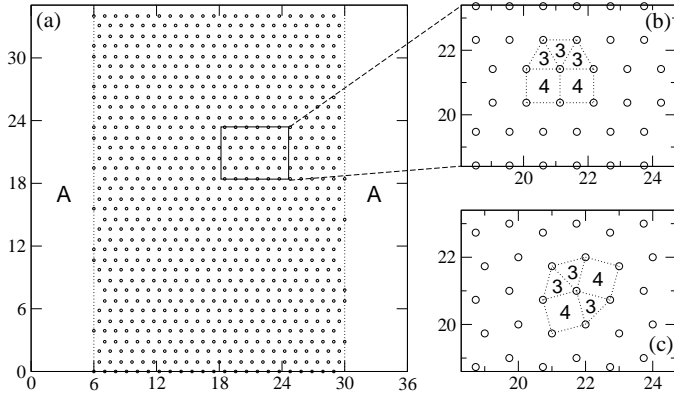


Figure 1. (a) The sample geometry shown with the $3^3 4^2$ pinning array. Circles represent pinning sites, and vortices are added in the unpinned regions marked A. (b,c) Pinning arrays constructed from Archimedean tilings. Plaquettes around one pinning site are highlighted with dotted lines, and labeled with the number of sides of the plaquette. The side numbers read off in a clockwise order around the pinning site are used to name the array. (b) The $3^3 4^2$ pinning array, also called an elongated triangular tiling. (c) The $3^2 4 3 4$ pinning array, also called a snub square tiling.

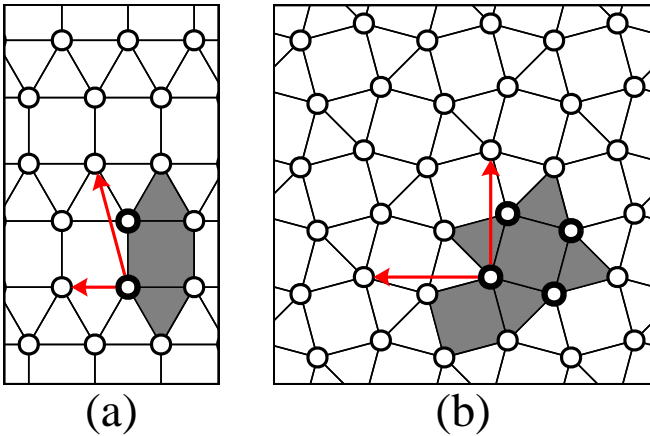


Figure 2. Bases for the various arrays. For each array, the pinning site basis generating the pinning array is plotted with thick dark circles, while the plaquette basis generating the tiling is indicated by the shaded polygons. Red arrows show the elementary translation vectors. (a) $3^3 4^2$ array. (b) $3^2 4 3 4$ array.

we place pinning sites at the vertices of the polygons to generate a pinning array. In figure 1(a) we illustrate the full simulation geometry for the $3^3 4^2$ pinning array. There are additional types of Archimedean tilings [35], but here we concentrate on only the two tilings illustrated in figure 1; pinning arrays constructed from other tilings will be described in a future work [30].

It might be expected that the behavior of the Archimedean pinning arrays would not differ significantly from that of purely square or triangular pinning arrays; however, we find that the different plaquette types in the Archimedean tilings compete. The triangular and square plaquettes comprising the array have equal side lengths a ; thus,

from simple geometry, the distance from the center of a plaquette to any of its vertices will be larger for the square plaquette ($a/\sqrt{2}$ versus $a/\sqrt{3}$). As a consequence, interstitial vortices prefer to occupy square plaquettes rather than triangular plaquettes. This produces several strong matching effects at certain non-integer filling fractions where the vortices are ordered, and suppresses commensurability effects at certain integer fillings where the vortices are disordered. In some cases we even find a drop in the pinning site occupancy with increasing magnetic field. We also observe several partially ordered states as well as different fractional fields and submatching fields that do not arise in regular square or periodic pinning arrays.

2. Simulation and System

In this work we utilize flux gradient density simulations as previously employed to study vortex pinning in random [31], periodic [32], and conformal pinning arrays [33]. The sample geometry is illustrated in figure 1(a). We consider a 2D system with periodic boundary conditions in the x - and y -directions. The sample size $36\lambda \times 36\lambda$ is measured in units of the penetration depth λ . Our previous studies indicate that this size of simulation box is sufficiently large to obtain experimentally relevant magnetization curves. The system represents a 2D slice of a three-dimensional type-II superconductor with a magnetic field applied in the perpendicular (\hat{z}) direction, and we assume that the vortices behave as rigid objects. We work in the London limit of vortices with pointlike cores, where the coherence length ξ is much smaller than λ . The pinning sites are located in a 24λ wide region in the middle portion of the sample, with pin-free regions labeled A in figure 1(a) on either side. Vortices are added to region A during the simulation, and their density in this region represents the externally applied field H . The vortices enter the pinned region from the edges and form a Bean gradient [36]. The motion of the vortices is obtained by integrating the following overdamped equation of motion:

$$\eta \frac{d\mathbf{R}_i}{dt} = \mathbf{F}_i^{vv} + \mathbf{F}_i^{vp}. \quad (1)$$

Here η is the damping constant which is set equal to 1, \mathbf{R}_i is the location of vortex i , \mathbf{F}_i^{vv} is the vortex-vortex interaction force, and \mathbf{F}_i^{vp} is the force from the pinning sites. The vortex-vortex interaction force is given by $\mathbf{F}_i^{vv} = \sum_{j \neq i} F_0 K_1(R_{ij}/\lambda) \hat{\mathbf{R}}_{ij}$, where K_1 is the modified Bessel function, $R_{ij} = |\mathbf{R}_i - \mathbf{R}_j|$, $\hat{\mathbf{R}}_{ij} = (\mathbf{R}_i - \mathbf{R}_j)/R_{ij}$, and $F_0 = \phi_0^2/(2\pi\mu_0\lambda^3)$, where ϕ_0 is the flux quantum and μ_0 is the permittivity. The pinning sites are modeled as N_p non-overlapping parabolic traps with $\mathbf{F}_i^{vp} = \sum_{k=1}^{N_p} (F_p R_{ik}^{(p)}/r_p) \Theta((r_p - R_{ik}^{(p)})/\lambda) \hat{\mathbf{R}}_{ik}^{(p)}$, where Θ is the Heaviside step function, $r_p = 0.12\lambda$ is the pinning radius, F_p is the pinning strength, $\mathbf{R}_k^{(p)}$ is the location of pinning site k , $R_{ik}^{(p)} = |\mathbf{R}_i - \mathbf{R}_k^{(p)}|$, and $\hat{\mathbf{R}}_{ik}^{(p)} = (\mathbf{R}_i - \mathbf{R}_k^{(p)})/R_{ik}^{(p)}$. We consider three pinning densities of $n_p = 1.0/\lambda^2$, $2.0/\lambda^2$, and $0.5/\lambda^2$, as well as a range of F_p values. All forces are measured in units of F_0 and lengths in units of λ . The magnetic field H is measured in terms of the matching field H_ϕ where the density of vortices equals the density of pinning sites. We measure only the first quarter of the magnetic hysteresis loop, which is sufficient to identify the

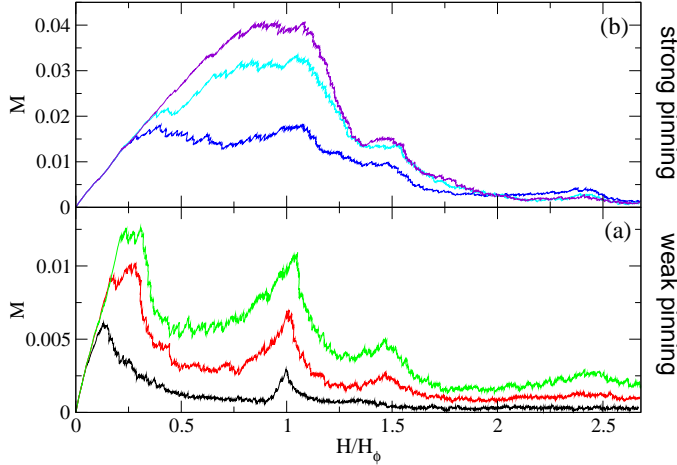


Figure 3. The magnetization M vs H/H_ϕ for the $3^3 4^2$ lattice from figure 1(b) with $n_p = 1.0/\lambda^2$. The various curves correspond to different values of the pinning strength F_p , which increases from bottom to top. (a) $F_p = 0.1$ (black), 0.2 (red), 0.3 (green). (b) $F_p = 0.5$ (blue), 0.8 (cyan), and 1.0 (violet).

different commensuration effects. We concentrate on the regime where only one vortex is trapped per pinning site, so that for fields greater than the first matching field, the additional vortices are located in the interstitial regions.

3. Elongated Triangular Tiling ($3^3 4^2$) Lattice

We first consider the elongated triangular tiling or $3^3 4^2$ lattice shown in figure 1(b), which consists of rows of square plaquettes separated by rows of triangular plaquettes. In figure 3 we plot the magnetization M vs H/H_ϕ , where $M = (1/4\pi V) \int (H - B) dV$ with B representing the field inside the pinned region and V its area. Here we use a pinning density of $n_p = 1.0/\lambda^2$. The critical current is proportional to the width of the magnetization loop, so a peak in M corresponds to a peak in the critical current. figure 3(a) shows M for $F_p = 0.1, 0.2$, and 0.3 . In each case there is a peak in M associated with the first matching condition of $H/H_\phi = 1.0$; however, at $H/H_\phi = 2.0$ there is no peak. Instead, peaks appear at $H/H_\phi = 1.5$ and 2.5 . In figure 3(b) we show M versus H/H_ϕ for samples with stronger pinning of $F_p = 0.5, 0.8$, and 1.0 . Here the peak at $H/H_\phi = 1.0$ is obscured by the initial rise in the magnetization; however, peaks are still present at $H/H_\phi = 1.5$ and 2.5 .

3.1. States at and above first matching field

In order to understand better the vortex states at fields beyond the first matching peak for both types of pinning arrays, we analyze the plaquette occupancy using the tiling coloring scheme illustrated in figure 4. In figure 4(a), we show a sample configuration of pinning sites and vortices for the $3^2 4^3 4$ lattice from Fig. 1(c). Figure 4(b) shows the same configuration represented as a plaquette occupancy diagram, with pinning

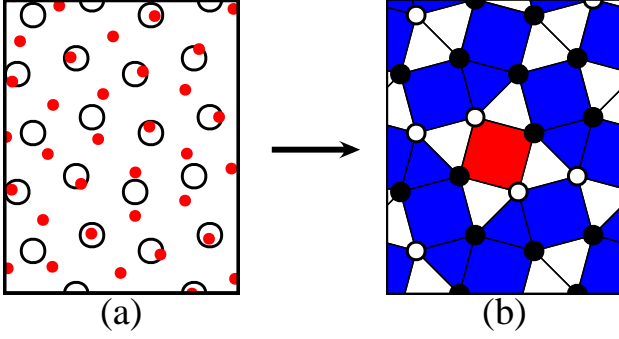


Figure 4. (a) Part of a sample vortex configuration in a $3^2 434$ array. Large open circles: pinning sites; small filled circles: vortices. (b) Corresponding plaquette occupancy diagram. Filled black circles denote occupied pinning sites, open circles denote empty pinning sites, and colored tiles indicate plaquettes occupied by one (blue) or more (red) interstitial vortices.

sites marked either dark or light depending on whether they are filled or empty, and plaquettes marked either with white fill, dark fill, or light fill depending on whether they are occupied by zero, one, or more than one interstitial vortex, respectively.

We focus on the field values at which peaks in M appear in figure 3. At $H/H_\phi = 1.0$, each pinning site captures one vortex, while at $H/H_\phi = 1.5$, the additional vortices predominantly occupy the interstitial regions at the center of the square plaquettes. This is shown in figure 5(a-c) where we plot the plaquette occupancy at $H/H_\phi = 1.55$ for increasing F_p . (We select a value of H/H_ϕ slightly higher than $H/H_\phi = 1.5$ to compensate for the Bean gradient since the field outside the pinning region is larger than the field inside the pinned part of the sample.) As F_p is increased, the ideal 1.5 state forms more cleanly. For the weak pinning situation $F_p = 0.2$ in figure 5(a), there are a handful of unoccupied pinning sites, and interstitial vortices occupy some triangular plaquettes and doubly occupy some of the square plaquettes. At $F_p = 0.5$ in figure 5(b), more of the pinning sites are filled and the interstitial vortices increasingly occupy only the square plaquettes. Finally, at strong pinning $F_p = 1.0$ in figure 5(c), nearly all pinning sites are occupied, since those vortices which were pinned at the first matching field never depin, so that as the field is raised above the first matching field, interstitial vortices enter the sample along the rows of square plaquettes, filling them. We note that there are a larger number of empty plaquettes at the center of the sample for the stronger pinning due to the Bean gradient, which is created by the pinning.

In figure 5(d,e,f) we show the plaquette fillings at $H/H_\phi = 2.56$ corresponding to the final peak in figure 3 for $F_p = 0.2, 0.5,$ and 1.0 , respectively. For the highest $F_p = 1.0$ in figure 5(f), all the pinning sites capture one vortex and most of the plaquettes are filled; however, in a number of locations there is an empty triangular plaquette accompanied by a doubly occupied square plaquette. At the weaker pinning strength $F_p = 0.2$ in figure 5(d), essentially all of the plaquettes, including the triangular ones, are filled; moreover, the weaker pinning leads to a number of unoccupied pinning sites. In these

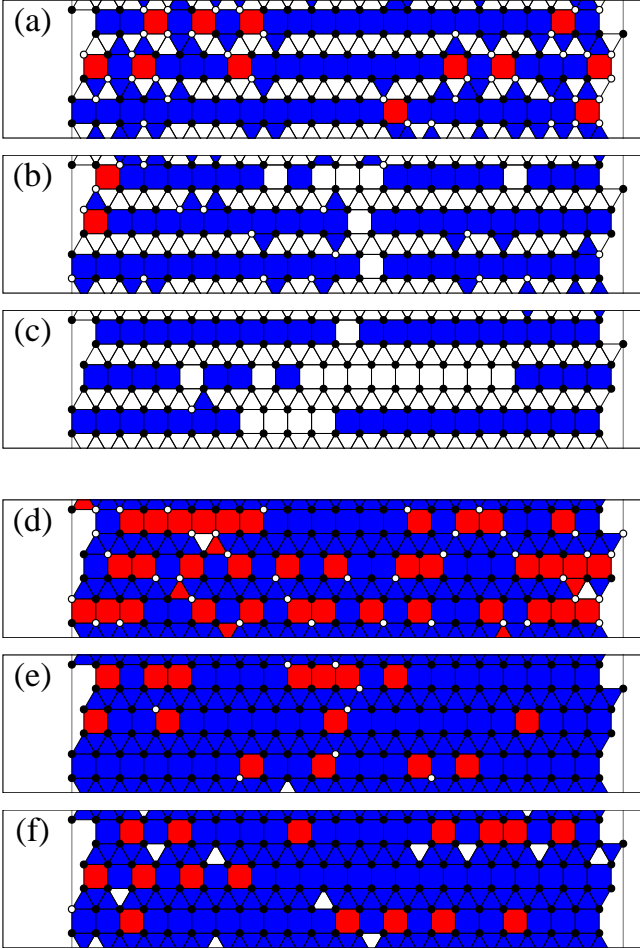


Figure 5. Plaquette occupancy in representative strips of the $3^3 4^2$ sample from figure 1(b), at field levels corresponding to peaks in figure 3. The full width of the pinned region is shown. The coloring scheme is described in figure 4. (a) $H/H_\phi = 1.55$, $F_p = 0.2$. (b) $H/H_\phi = 1.55$, $F_p = 0.5$. (c) $H/H_\phi = 1.55$, $F_p = 1.0$. At this field the square plaquettes are predominantly filled. (d) $H/H_\phi = 2.56$, $F_p = 0.2$. (e) $H/H_\phi = 2.56$, $F_p = 0.5$. (f) $H/H_\phi = 2.56$, $F_p = 1.0$. At this field most plaquettes are filled.

cases the depinned vortices prefer to sit in the square plaquettes, making them doubly occupied.

At $H/H_\phi = 2.0$ the system could in principle form an ordered state where every square plaquette is occupied while every other triangular plaquette is unoccupied; however, we do not observe such an ordered state. Instead, we find that as the field is increased from the ordered $H/H_\phi = 1.5$ state where only the square plaquettes are occupied, some pinned vortices are pushed out of the pinning sites when additional vortices try to occupy the triangular plaquettes. As a result, the pin occupancy actually decreases with increasing field, as shown in figure 6(a) where we plot the fraction of occupied pinning sites P versus H/H_ϕ for the $3^3 4^2$ system at four different values of F_p . There is a peak in P just above $H/H_\phi = 1.0$ corresponding to the first matching field

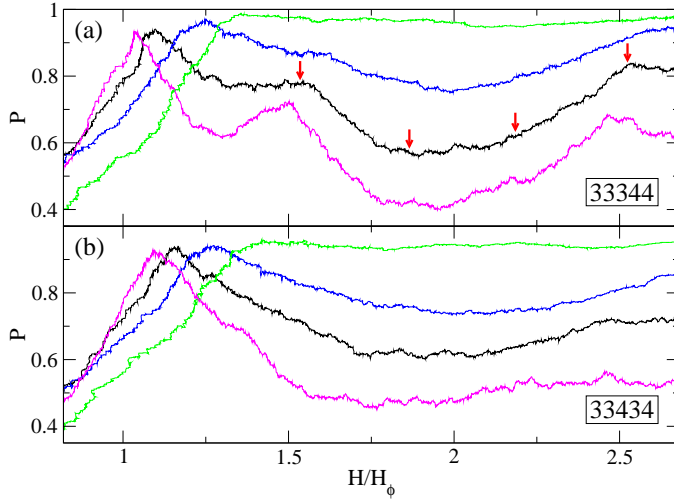


Figure 6. P , the fraction of occupied pins, vs H/H_ϕ . (a) The $3^3 4^2$ array from figure 3 at $F_p = 0.2, 0.3, 0.5$, and 0.8 , from bottom right to top right. Arrows pointing to various locations on the $F_p = 0.3$ curve indicate field levels where we illustrate the real-space vortex configurations in figure 7. (b) The $3^2 4^3 4$ array at $F_p = 0.2, 0.3, 0.5$, and 0.8 , from bottom right to top right.

where most of the pinning sites are occupied. For weaker pinning, $F_p \leq 0.5$, P declines from its peak but stabilizes near $H/H_\phi = 1.5$, as illustrated for $F_p = 0.3$ in figure 6(a). As H/H_ϕ increases further, P begins to fall substantially when vortices start to push their way into triangular plaquettes, causing the vortices at the neighboring pinning sites to depin. Near $H/H_\phi = 2.0$, P passes through a minimum; the overall vortex configuration at $H/H_\phi = 2.0$ is disordered and there is no peak in M at this field. P then recovers and increases up to the ordered state at $H/H_\phi = 2.5$, where every square and every triangular plaquette can contain an interstitial vortex as illustrated in figure 5(d,e). The field level for this state can be understood from figure 2(a), where we see that a basis for the $3^3 4^2$ tiling has 2 pinning sites, 2 triangular plaquettes, and 1 square plaquette; if all these are singly occupied, we obtain a field level of $5/2 = 2.5$.

It is instructive to visualize the transition from $H/H_\phi = 1.5$ to $H/H_\phi = 2.5$ in real space. After the first matching field is reached and the pinning sites become occupied, interstitial vortices enter the sample between the square tiles in neat horizontal lines. This continues until every square tile in a row contains one interstitial vortex, giving the $H/H_\phi = 1.5$ state shown in figure 7(a). When further vortices attempt to enter, the lines of interstitials buckle, as shown in figure 7(b,c); in this process, many pinned vortices are dislodged, and the triangular plaquettes become filled in an irregular manner. As the sample approaches the ordered $H/H_\phi = 2.5$ state, the lines of interstitial vortices re-form along the square plaquettes, and the triangular plaquettes now also fill with lines of interstitials which zig-zag due to the alternating orientation of the triangles. This is illustrated in figure 7(d).

For stronger pinning $F_p > 0.5$, the pinned vortices do not depin when the triangular plaquettes start to become occupied around $H/H_\phi = 2.0$, as shown for $F_p = 0.8$ in figure

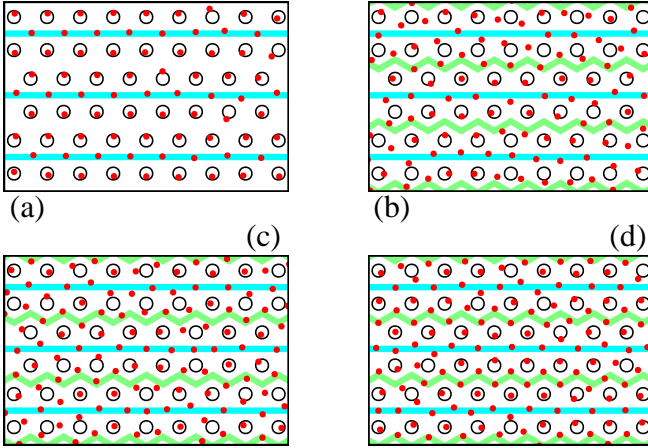


Figure 7. Real space images of vortex configurations for the $3^3 4^2$ array at $F_p = 0.3$ as the field H/H_ϕ is increased from 1.5 to 2.5, showing lines of interstitial vortices buckling and then reforming. Open circles: pinning sites; filled dots: vortices; thick lines: guides to the eye running along rows of plaquettes and connecting their centers, which are preferred locations for interstitial vortices when all surrounding pinning sites are occupied. (a) $H/H_\phi = 1.535$; (b) 1.865; (c) 2.185; (d) 2.524. The field levels shown correspond to the red arrows in figure 6(a).

6(a); thus, the buckling phenomenon observed for weaker pinning does not occur in this case. However, the vortex configurations around $H/H_\phi = 2.0$ are still disordered even for strong pinning, since the triangles do not become occupied in an orderly manner.

3.2. Submatching states

We also find vortex ordering at some submatching fields for the $3^3 4^2$ pinning array. This is more clearly visible in an array with higher density $n_p = 2.0/\lambda^2$ and small F_p . In figure 8(a) we plot P_4 , the fraction of vortices with a coordination number of four, versus H/H_ϕ for samples with $3^3 4^2$ pinning arrays with $F_p = 1.0, 0.5,$ and 0.2 . We obtain the coordination number z_i of each vortex using a Voronoi construction of the vortex positions, and take $P_4 = N_v^{-1} \sum_{i=1}^{N_v} \delta(4 - z_i)$. For $F_p = 0.2$ there is a peak in P_4 just above $H/H_p = 0.5$, marked with an arrow in figure 8(a), which corresponds to an ordered vortex sub-matching configuration. This configuration is illustrated in figure 8(c), where we show the locations of the vortices and pinning sites and add a thick line between pairs of occupied pinning sites to make the ordering more visible. Here, every other pinning site captures a vortex and there is an effective dimerization of the occupied pinning sites along the edges of the triangular plaquettes. The dimers are tilted 30° from the y axis in one row and -30° from the y axis in the next row, giving a herringbone ordering of the type previously studied for dimer molecules adsorbed on triangular substrates [34]. As the pinning strength increases, the dimer ordering breaks apart. For the $3^2 4^3 4$ array there is no herringbone ordering, as shown by the absence of a peak in P_4 in figure 8(b).

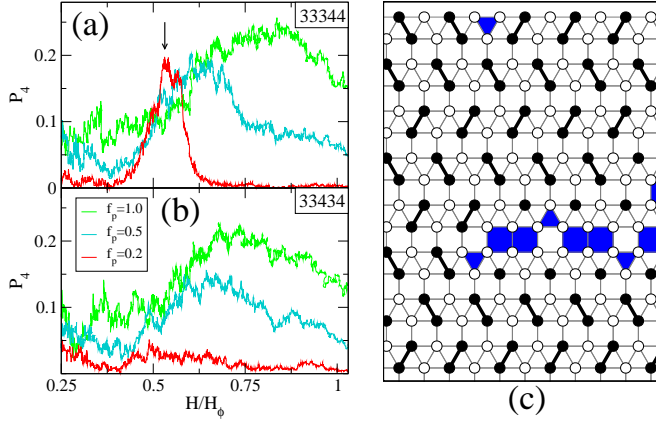


Figure 8. (a) P_4 , the fraction of vortices with a coordination number of 4, vs H/H_ϕ for the 3^34^2 array in a system with $n_p = 2.0/\lambda^2$ and $F_p = 0.2$ (blue), 0.5 (red) and 1.0 (green). Here a peak (marked with an arrow) occurs near $H/H_\phi = 0.5$ for the weakest pinning. (b) P_4 vs H/H_ϕ for the 3^2434 array at $n_p = 2.0/\lambda^2$ and $F_p = 0.2$ (blue), 0.5 (red) and 1.0 (green); the peak from panel (a) is absent. (c) A subsection of the $F_p = 0.2$ system in the 3^34^2 sample from panel (a) at $H/H_\phi = 0.5$. Empty circles: unoccupied pinning sites; filled circles: occupied pinning sites; white squares and triangles: unoccupied square and triangular plaquettes; filled squares and triangles: square and triangular plaquettes that each contain one vortex. A thick heavy line is drawn between pairs of occupied pinning sites to highlight the herringbone ordering.

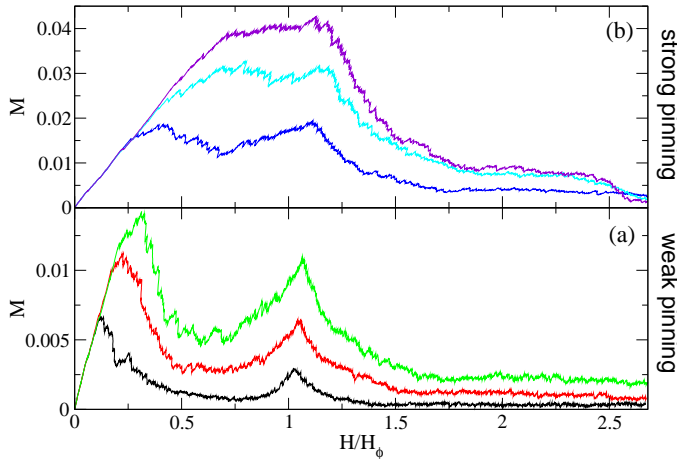


Figure 9. M vs H/H_ϕ for the 3^2434 array from figure 1(c) for $n_p = 1.0/\lambda^2$. (a) $F_p = 0.1$ (black), 0.2 (red), and 0.3 (green). (b) The same for $F_p = 0.5$ (blue), 0.8 (cyan) and 1.0 (violet).

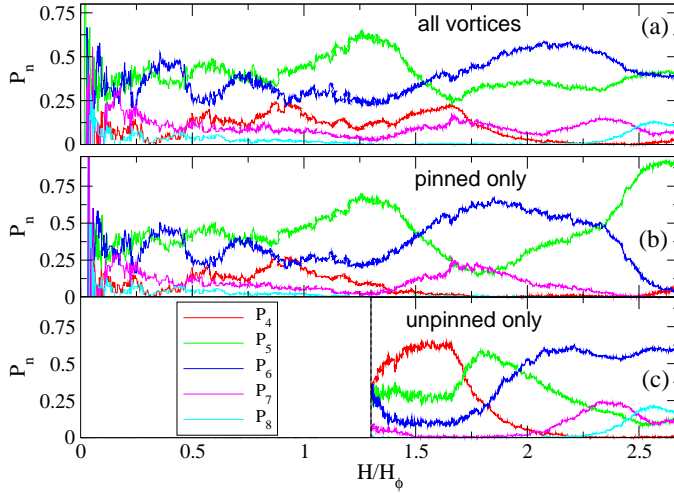


Figure 10. P_n vs H/H_ϕ for the $3^2 434$ array at $F_p = 1.0$, with P_4 (red), P_5 (green), P_6 (blue), P_7 (violet) and P_8 (cyan). (a) All vortices in the system. (b) Pinned vortices only. (c) Unpinned vortices only. Below $H/H_\phi = 1.25$ (shaded region in panel (c)), there are too few unpinned vortices to give a clear signal.

4. Snub Square ($3^2 434$) Tiling

We next consider the the snub square tiling or $3^2 434$ pinning array illustrated in figure 1(c). In figure 9(a) we plot M vs H/H_ϕ for this array with $F_p = 0.1, 0.2,$ and 0.3 , while samples with $F_p = 0.5, 0.8,$ and 1.0 are shown in figure 9(b). Here a matching peak occurs at $H/H_\phi = 1.0$ but there are no other clearly defined peaks at the higher fillings. For the stronger pinning sample with $F_p = 1.0$, the first matching peak is obscured by the initial rise of M as shown in figure 9(b). Since there are few additional features in M , we use alternative measurements to show that a variety of partially ordered vortex states can occur in this system. In particular, we consider the fraction of n -fold coordinated vortices P_n , with $n = 4, 5, 6, 7,$ and 8 , defined as written earlier for P_4 .

In figure 10(a) we plot P_n with $n = 4$ through 8 versus H/H_ϕ for all the vortices in a $3^2 434$ sample with strong pinning $F_p = 1.0$. The ordered states in this system can be more easily distinguished by separately measuring P_n for the pinned vortices only, shown in figure 10(b), and for the interstitial or unpinned vortices only, shown in figure 10(c). In particular, in figure 10(c) we find successive peaks in $P_{4,5,6,7,8}$ for the interstitial vortices. Since there are few to no interstitial vortices for $H/H_\phi < 1.25$, we do not show P_n for this field range in figure 10(c). The first peak in P_n for the interstitial vortices appears in P_4 just above $H/H_\phi = 1.5$ in figure 10(c). Here, most of the pinning sites are occupied and the interstitial vortices primarily sit in the square plaquettes, as indicated in the plaquette occupancy plot in figure 11(a) for $H/H_\phi = 1.65$. An interstitial vortex in a square plaquette has four nearest neighbors, the pinned vortices at the edges of the plaquette. As the field increases, interstitial vortices begin to occupy isolated triangular plaquettes, providing an additional nearest neighbor for the interstitial vortices in the nearby square plaquettes. This produces a peak in P_5 at $H/H_\phi = 1.79$ in figure 10(c),

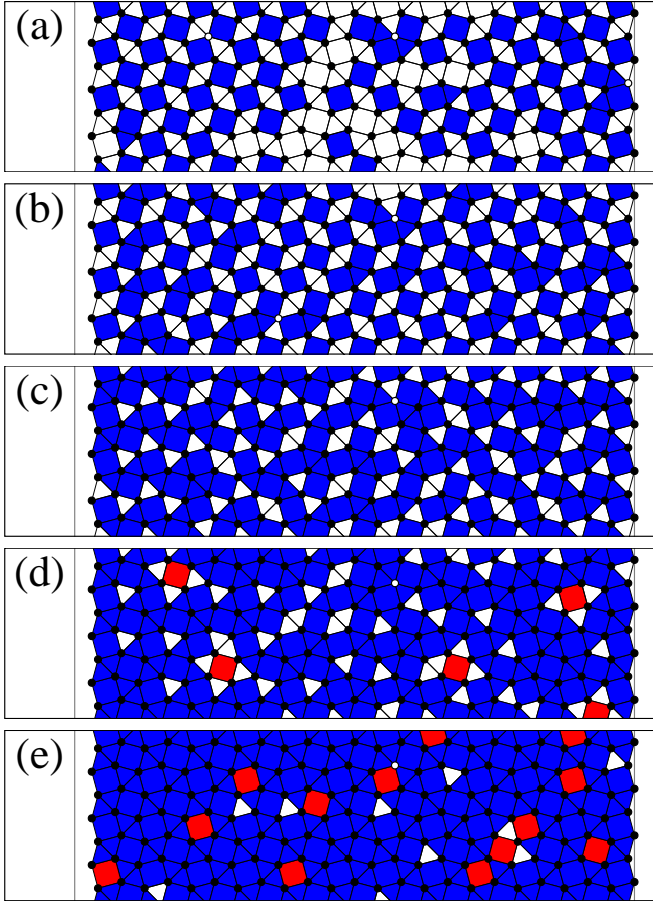


Figure 11. Plaquette occupancy in representative strips of the samples for the $3^2 4^3 4$ array with $F_p = 1.0$, at field levels corresponding to peaks in figure 10(c). The full width of the pinned region is shown. The coloring scheme is described in figure 4. (a) $H/H_\phi = 1.65$, (b) 1.79, (c) 2.08, (d) 2.33, and (e) 2.56.

where nearly all of the filled square plaquettes have one neighboring filled triangular plaquette as shown in figure 11(b). At $H/H_\phi = 2.08$, there is a peak in P_6 in figure 10(c), and the corresponding configuration in figure 11(c) shows that many of the square plaquettes now have two neighboring filled triangular plaquettes. A peak in P_7 appears at $H/H_\phi = 2.33$ in figure 10(c), and the configuration in figure 11(d) has many square plaquettes with three neighboring filled triangular plaquettes, as well as a few doubly occupied square plaquettes. Finally, at $H/H_\phi = 2.56$ there is a peak in P_8 in figure 10(c). The corresponding configurations in figure 11(e) indicate that most of the plaquettes are now filled, with some empty triangular plaquettes and some doubly occupied square plaquettes.

We can understand the field levels at which the peaks in P_n occur by considering figure 2(b), where we illustrate both the pinning site basis and the plaquette basis which generate the $3^2 4^3 4$ tiling. In a ground state configuration at $H/H_\phi = 1.0$, there are four vortices occupying the four pins comprising the basis, with no interstitial vortices. For the state where each square plaquette is occupied by one interstitial vortex, there

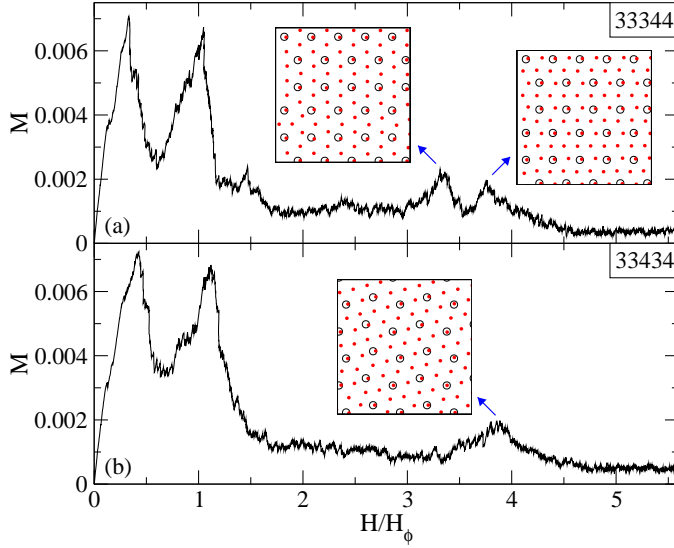


Figure 12. M vs H/H_ϕ for samples with $n_p = 0.5/\lambda^2$ and $F_p = 0.3$. (a) In the $3^3 4^2$ array, there are additional peaks at $H/H_\phi = 3.5$ and 4.0 . Insets: the ordered vortex arrangements that appear at these additional peaks, indicated by arrows. In the insets, the open circles are pinning sites and the filled circles are vortices. (b) In the $3^2 4^3 4$ array, there is a peak at $H/H_\phi = 3.75$; the inset shows the ordered vortex arrangement that forms at this field. In the inset, the open circles are pinning sites and the filled circles are vortices.

are a total of 6 vortices per basis compared to 4 pins; so the field for this state is $H/H_\phi = 6/4 = 1.5$. Each of the interstitial vortices sitting in a square plaquette has 4 nearest neighbors, the pinned vortices at the corners of the square. As H/H_ϕ increases further, the triangular plaquettes become occupied one by one, with each new triangular plaquette interstitial providing an additional nearest neighbor for a nearby square plaquette interstitial vortex. This process gives a total of 7, 8, 9, or 10 vortices per basis leading to fields of $H/H_\phi = 1.75, 2.0, 2.25,$ and 2.5 , respectively. Thus, the peaks in $P_4, P_5, P_6, P_7,$ and P_8 for the unpinned vortices in figure 10(c) arise simply from the coordination numbers of the interstitial vortices occupying the square plaquettes. The actual peaks from the simulation shown in figure 10(c) occur at $H/H_\phi = 1.65, 1.79, 2.08, 2.33,$ and 2.56 , which are close to the ideal field values. The small shift in the actual values is due to the flux gradient and also to the occasional double occupancy of square plaquettes found in figure 11(d,e). The peaks in P_n for the pinned vortices shown in figure 10(b) follow immediately from the behavior of the interstitial vortices described above. We note in particular that P_5 becomes nearly one at $H/H_\phi = 2.5$, since almost all the triangular and square plaquettes are occupied as shown in figure 11(e). Since each pinning site is surrounded by 5 plaquettes, the nearest neighbors of each pinned vortex are surrounded by 5 interstitial vortices at this filling.

5. Smaller Pinning Densities

For the case of a pinning density of $n_p = 0.5/\lambda^2$ and smaller F_p we can readily observe matching peaks up to $H/H_\phi = 5.0$. In figure 12(a) we plot M vs H/H_ϕ for the 3^34^2 array at $F_p = 0.3$ and in figure 12(b) we show the same quantity for the 3^2434 pinning array. In the 3^34^2 array, we find the same peaks shown in figure 3 at $H/H_\phi = 1.0, 1.5,$ and $2.5,$ and we observe additional peaks just below $H/H_\phi = 3.5$ and 4.0 . In the insets of figure 12(a) we plot the vortex and pinning site locations at the two new peaks at $H/H_\phi = 3.5$ and 4.0 . Here, all of the pinning sites are occupied and an ordered crystalline arrangement of vortices occurs. By directly counting the number of vortices per pinning site in the ordered part of the sample, we confirm that these are the 3.5 and 4.0 fillings. For the 3^2434 array, figure 12(b) shows a peak in M for $H/H_\phi = 3.75$ corresponding to the ordered vortex array illustrated in the inset.

6. Summary

We have investigated ordering and pinning of vortices interacting with Archimedean pinning arrays. The arrays are constructed using the vertices of Archimedean tilings of squares and triangles, and we specifically examine the elongated triangular tiling and the snub square tiling. For the elongated triangular or 3^34^2 array, we find that beyond the first matching field, the interstitial vortices first fill the square plaquettes and subsequently fill the triangular plaquettes, producing pronounced peaks in the magnetization at noninteger matching fields along with an absence of peaks at certain higher integer matching fields. The competition between filling the more confined triangular plaquettes with single vortices or doubly occupying the larger square plaquettes can lead to a decrease in the fraction of occupied pins as the field is increased, and can produce disordered vortex states at certain integer matching fields. We also find novel vortex orderings at submatching fillings, such as herringbone configurations for weak pinning. For the snub square or 3^2434 array above the first matching field, we find that by analyzing the plaquette fillings we can correctly predict the appearance of a sequence of partially ordered states, where interstitial vortices first occupy square plaquettes and then fill the triangular plaquettes. At higher fields we observe additional commensuration effects at noninteger matching fields which correspond to ordered vortex structures. Our results can be tested for experiments on Archimedean tiling pinning arrays in superconductors as well as for colloids interacting with optical trap arrays with similar geometries.

7. Acknowledgments

This work was carried out under the auspices of the NNSA of the U.S. DoE at LANL under Contract No. DE-AC52-06NA25396.

References

- [1] Fiory A T, Hebard A F and Somekh S 1978 *Appl. Phys. Lett.* **32** 73
- [2] Baert M, Metlushko V V, Jonckheere R, Moshchalkov V V, and Bruynseraede Y 1995 *Phys. Rev. Lett.* **74** 3269
- [3] Metlushko V, Welp U, Crabtree G W, Osgood R, Bader S D, DeLong L E, Zhang Z, Brueck S R J, Ilic B, Chung K and Hesketh P J 1999 *Phys. Rev. B* **60** R12585
- [4] Martín J I, Vélez M, Nogués J and Schuller I K 1997 *Phys. Rev. Lett.* **79** 1929
- [5] Welp U, Xiao Z L, Jiang J S, Vlasko-Vlasov V K, Bader S D, Crabtree G W, Liang J, Chik H and Xu J M (2002) *Phys. Rev. B* **66** 212507
- [6] Goldberg S, Segev Y, Myasoedov Y, Gutman I, Avraham N, Rappaport M, Zeldov E, Tamegai T, Hicks C W and Moler K A (2009) *Phys. Rev. B* **79** 064523
- [7] Thakur A D, Ooi S, Chockalingam S P, Jesudasan J, Raychaudhuri P and Hirata K (2009) *Appl. Phys. Lett.* **94** 262501
- [8] Swiecicki I, Ulysse C, Wolf T, Bernard R, Bergeal N, Briatico J, Faini G, Lesueur J and Villegas J E (2012) *Phys. Rev. B* **85** 224502
- [9] Harada K, Kamimura O, Kasai H, Matsuda T, Tonomura A and V.V. Moshchalkov V V (1996) *Science* **274** 1167
- [10] Reichhardt C, Olson C J and Nori F (1998) *Phys. Rev. B* **57** 7937
- [11] Berdiyrov G R, Milosevic M V and Peeters F M (2006) *Phys. Rev. Lett.* **96** 207001
- [12] Karapetrov G, Fedor J, Iavarone M, Rosenmann D and Kwok W-K (2005) *Phys. Rev. Lett.* **95** 167002
- [13] Baert M, Metlushko V V, Jonckheere R, Moshchalkov V V and Bruynseraede Y (1995) *Europhys. Lett.* **29** 157
- [14] Reichhardt C and Grønbech-Jensen N (2001) *Phys. Rev. B* **63** 054510
- [15] Field S B, James S S, Barentine J, Metlushko V, Crabtree G, Shtrikman H, Ilic B and Brueck S R J (2002) *Phys. Rev. Lett.* **88** 067003
- [16] Grigorenko A N, Bending S J, Van Bael M J, Lange M, Moshchalkov V V, Fangohr H and de Groot P A J (2003) *Phys. Rev. Lett.* **90** 237001
- [17] Ooi S, Mochiku T and Hirata K (2009) *Physica C* **469** 1113
- [18] Martín J I, Vélez M, Hoffmann A, Schuller I K and Vicent J L (1999) *Phys. Rev. Lett.* **83** 1022
- [19] Reichhardt C, Zimányi G T and Grønbech-Jensen N (2001) *Phys. Rev. B* **64** 014501
- [20] Morgan D J and Ketterson J B (1998) *Phys. Rev. Lett.* **80** 3614
- [21] Wu T C, Wang J C, Horng L, Wu J C and Yang T J (2005) *J. Appl. Phys.* **97** 10B102
- [22] Reichhardt C and Olson Reichhardt C J (2007) *Phys. Rev. B* **76** 064523
- [23] Cao R, Horng L, Wu T C, Wu J C and Yang T J (2009) *J. Phys.: Condens. Matter* **21** 075705
- [24] Latimer M L, Berdiyrov G R, Xiao Z L, Kwok W K and Peeters F M (2012) *Phys. Rev. B* **85** 012505
- [25] Reichhardt C and Olson Reichhardt C J (2007) *Phys. Rev. B* **76** 094512
- [26] Kemmler M, Bothner D, Ilin K, Siegel M, Kleiner R and Koelle D (2009) *Phys. Rev. B* **79** 184509
- [27] Libál A, Olson Reichhardt C J and Reichhardt C (2009) *Phys. Rev. Lett.* **102** 237004
- [28] Silhanek A V, Van Look L, Jonckheere R, Zhu B Y, Raedts S and Moshchalkov V V (2005) *Phys. Rev. B* **72** 014507
- [29] Horng L, Cao R, Wu T-C, Yang S, Wang S-H, Wu J-C and Yang T-J (2013) *J. Appl. Phys.* **113** 17E118
- [30] Ray C, Reichhardt C and Olson Reichhardt C J, unpublished.
- [31] Reichhardt C, Olson C J, Groth J, Field S and Nori F (1995) *Phys. Rev. B* **52** 10441
- [32] Reichhardt C, Groth J, Olson C J, Field S B and Nori F (1996) *Phys. Rev. B* **54** 16108
- [33] Ray D, Olson Reichhardt C J, Jankó B and Reichhardt C (2013) *Phys. Rev. Lett.* **110** 267001
- [34] Nicol E J, Kallin C and Berlinsky A J (1988) *Phys. Rev. B* **38** 556
- [35] Grünbaum B and Shephard G C *Tilings and Patterns* (W.H.Freeman, New York, 1987), Ch. 2.

- [36] Bean C P (1962) *Phys. Rev. Lett.* **8** 250; (1964) *Rev. Mod. Phys.* **36** 31